Biosensors and Bioelectronics 26 (2010) 207–212

Contents lists available at ScienceDirect

Biosensors and Bioelectronics

journal homepage: www.elsevier.com/locate/bios

Arrayed CNT–Ni nanocomposites grown directly on Si substrate for amperometric detection of ethanol

Yan-Shi Chen, Jin-Hua Huang*

Department of Materials Science and Engineering, National Tsing Hua University, 101, Sec. 2, Kuang-Fu Road, Hsinchu 300, Taiwan

ARTICLE INFO

Article history:
Received 3 April 2010
Received in revised form 5 June 2010
Accepted 11 June 2010
Available online 20 June 2010

Keywords:
Ni nanoparticles
CNT
Ethanol sensor

ABSTRACT

A novel amperometric biosensor utilizing carbon nanotube (CNT)–Ni nanoparticle hybrid arrays for ethanol detection has been developed. The sensor was fabricated by e-beam deposition of thin Ni film on arrayed multi-walled carbon nanotubes grown directly on Si substrate. As the Ni film thickness is ≤200 nm, high-resolution SEM and TEM images showed well-dispersed and strongly adhered crystalline Ni nanoparticles uniformly populated on the sidewalls of CNTs, and the sensitivity of the resultant CNT–Ni sensor generally increased with increasing nickel thickness. The best sensor showed a wide response range of 50–600 μM, a response time of <10 s, and a sensitivity of 14.81 μA μM^{-1} cm^{-2} which is ~380% higher in comparison with the nanostructured Ni/Pt/Ti electrodes.

1. Introduction

Ethanol sensors with high sensitivity, selectivity, and short response time are needed for many applications, such as in medicine, fermentation, and food industry. Accurate and reliable measurement of ethanol is also very important in clinical, agricultural, and environmental analyses. Conventional analytical methods, such as chromatography, spectrometry, and refractometry, often require relative expensive instruments which are laborious, complex, and time-consuming to operate. Thus, much progress has been made in finding a more cost-effective approach of using electrochemical biosensors with enzyme-modified electrodes. The enzymatic biosensors were commonly fabricated by attaching either alcohol oxidase (AOD) (Xie et al., 1992; Vijayakumar et al., 1996) or alcohol dehydrogenase (ADH) (Wang et al., 1992; Katrlik et al., 1998) to suitable solid electrodes, which catalyze the conversion of alcohol to aldehyde. In the case of AOD-based biosensors, the consumption of O_2 or the production of H_2O_2 is measured, while the ADH-based biosensors rely upon the electrocatalytic ability toward the NADH in the presence of coenzyme nicotinamide adenine dinucleotide (NAD^+). However, the enzyme-modified electrodes have several constraints, such as short lifetime, poor stability, and susceptible to temperature change.

To overcome the disadvantages of enzymatic methods mentioned above, electrodes based on pure nickel or nickel-coated substrates have appeared to be promising alternatives for electrochemical ethanol sensing (Liao and Chou, 2000; Pang et al., 2001; Weng et al., 2004). The ethanol detection mechanism of nickel-based electrodes is based on the oxidation of ethanol, at a lower electrocatalyzed potential, by the redox pair of $Ni(OH)_2$/NiOOH on nickel surface in alkaline media (Sattar and Conway, 1969; Carbonio et al., 1982; Lo and Hwang, 1995). However, these two-dimensional plate-type nickel electrodes provide relatively insufficient surface area and thus showed marginal catalytic activity towards the oxidation of ethanol (Liao and Chou, 2000; Pang et al., 2001). Nevertheless, the sensing performance of the Ni-based electrochemical sensors had been considerably improved by increasing surface area of the electrodes by using nanostructured nickel (Weng et al., 2004).

Due to the high surface free energy provided by their enormous surface areas, many kinds of metal nanoparticles exhibit excellent catalytic properties and have been widely used in electrochemical sensors and biosensors (Luo et al., 2006). On the other hand, many studies have revealed that carbon nanotubes (CNTs) is an outstanding catalyst support (Fang et al., 2007) due to its high surface area and excellent electron transfer rate (Nugent et al., 2001). Furthermore, vertically aligned CNTs can act as molecular wires to allow efficient electron transfer between the underlying electrode and the redox centers (Wang, 2005). There are many active efforts to develop a variety of electrochemical sensors with hybrid nanoparticles/CNTs materials. For example, gold (Manso et al., 2007), palladium (Lee et al., 2007; Lim et al., 2005), platinum (Tang et al., 2004), and CdTe (Liu et al., 2007) nanoparticles have been used in conjunction with CNTs for the electrocatalytic sensing of glucose. The as-produced nanocomposites have demonstrated electrochemical and sensing performances superior to their bulk counterparts. Thus, hybrid nanocomposites constructed by modifying the surface of arrayed CNTs with well-dispersed Ni nanoparticles is expected to be a promising catalyst material for

* Corresponding author. Tel.: +886 3 5162228; fax: +886 3 5722366.
E-mail address: jihhuang@mx.nthu.edu.tw (J.-H. Huang).

0956-5663/$ – see front matter © 2010 Elsevier B.V. All rights reserved.
doi:10.1016/j.bios.2010.06.016

ethanol detection. The Ni–CNT nanocomposites have been produced by electro deposition (Arai et al., 2004; Jin et al., 2007), electroless deposition (Wang et al., 2005), or impregnation (Kim et al., 2005). However, due to the insolubility of CNTs in all solvents, wet chemical pretreatments and/or metal organic precursors were commonly utilized to obtain dispersed Ni nanoparticles on CNTs in those studies. In this work, we present a simple yet efficient route for the preparation of well-dispersed Ni nanoparticles on vertically aligned CNTs grown directly on Si substrates. It is found that well-dispersed Ni nanoparticles can be formed on the sidewalls of CNTs by e-beam deposition without using any wet chemical pretreatments or metal organic precursors. The resulting CNT–Ni nanocomposite showed a sensitivity of up to 14.81 $\mu A\,\mu M^{-1}\,cm^{-2}$ with a response time of <10 s.

2. Experimental

2.1. Preparation of arrayed CNT–Ni nanocomposites

Prior to CNT growth, chromium (Cr), titanium (Ti), and cobalt (Co) metals with thicknesses of 100, 40, and 8 nm, respectively, were consecutively deposited onto a SiO_2/Si substrate of an area of 2 cm^2 by e-beam evaporation. Then, aligned multi-walled carbon nanotubes were grown by microwave-heated chemical vapor deposition (MH-CVD) (Huang et al., 2005). The MH-CVD growth of CNTs was carried out at a microwave power of 1100 W, a substrate temperature of 680 °C, and a growth time of 15 min. Only CH_4 was fed into the deposition chamber, and the chamber pressure was maintained at 1 atm. The deposited Cr/Ti bilayer was used to improve the adhesion and reduce the contact resistance between the CNTs and the Si substrate. Finally, Ni with thickness of 60–240 nm was deposited on the CNT arrays using e-beam evaporation in a vacuum of $\sim 10^{-7}$ Torr. To ensure the deposited Ni is in the form of nanoclusters, the deposition rate of Ni was kept as slow as 0.1–0.5 Å/s.

2.2. Characterization

The surface morphology of the arrayed CNT–Ni nanocomposites was characterized by field-emission scanning electron microscopy (FESEM). The detailed nanostructure of the hybrid nanocomposites was studied by use of high-resolution transmission electron microscopy (TEM). The electrochemical (EC) behaviors of the CNT–Ni nanocomposites were characterized by cyclic voltammetry and chronoamperometry using an EG&G 273 potentiostat. In addition, high-resolution X-ray photoelectron spectroscopy (HRXPS) was employed to investigate the states of $Ni(OH)_2$/NiOOH before and after the EC sensing of ethanol.

2.3. Sensing system

The sensing system contained a three-electrode cell using the fabricated CNT–Ni hybrid nanocomposites (area of 0.16 cm^2) as the working electrode, platinum wire as the counter electrode, and Ag/AgCl (saturated KCl) as the reference electrode. All operational potential values given below refer to Ag/AgCl. Amperometric measurements were carried out under steady-state conditions in a 0.5 M KOH aqueous solution by applying a desired potential within the limiting current window of the working electrode. When the background current had achieved a steady-state value, 50 μM of ethanol (or other interfering species) was added and the new steady-state current was noted. With each addition, the response current increased and a new steady-state was reached. The differences between these currents and the background current were used to construct a calibration curve for concentration of ethanol versus response current. The sensitivities of the CNT–Ni sensors were calculated using the equation

$$S = \frac{\Delta I}{\Delta C \times A},$$

where S is the sensitivity in $\mu A/(\mu M\,cm^2)$, ΔI is the current response in μA, ΔC is the difference of ethanol concentration in μM, and A is the surface area of the CNT–Ni electrode in cm^2.

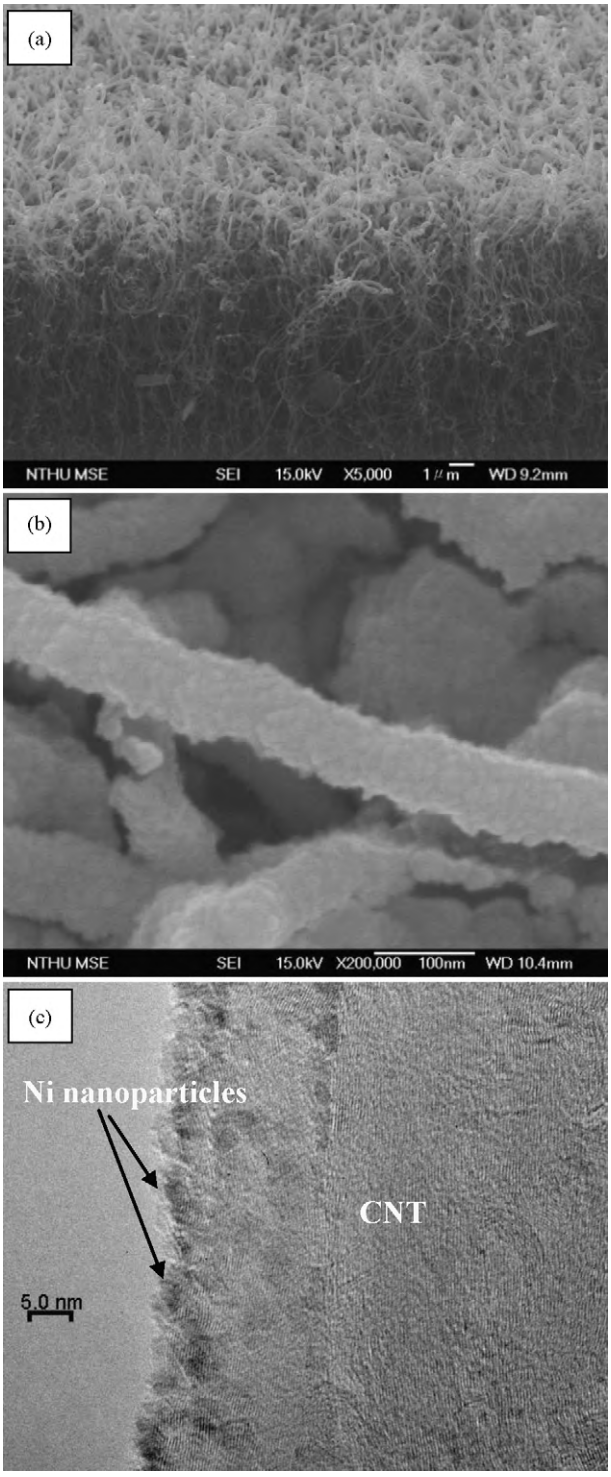

Fig. 1. (a) Low-magnification cross-sectional and (b) high-magnification top-view FESEM micrographs of CNTs with 100 nm Ni coating. (c) High-resolution TEM image showing dispersed nanonickel crystallites.

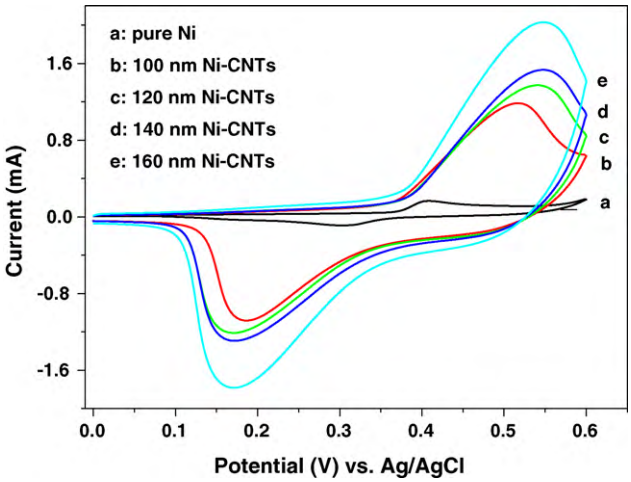

Fig. 2. Cyclic voltammograms of different electrodes including (a–d) 100–160 nm Ni modified CNTs and (e) pure Ni. The curves were taken in 0.5 M KOH solution at a scan rate of 40 mV/s.

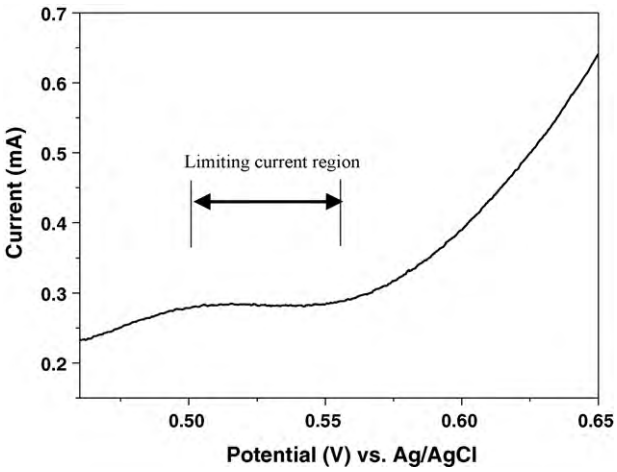

Fig. 3. Linear sweep voltammogram of the CNT–Ni nanocomposite with 100 nm Ni thickness. The curve was taken in a solution of 1 mM ethanol in 0.5 M KOH. Scan rate: 1 mV/s.

3. Results and discussion

3.1. Structural characterization

Fig. 1 shows the FESEM and TEM images of CNTs after the e-beam deposition of 100 nm Ni. The low-magnification cross-sectional FESEM image, Fig. 1(a), demonstrates arrayed nanocomposites with average length ~10 μm grow vertically to the substrate. The high-magnification FESEM image, Fig. 1(b), illustrates that nickel nanoclusters have coated on the surface of CNTs with good uniformity and conformity. Additionally, the high-resolution TEM micrograph in Fig. 1(c) depicts that nickel nanoparticles as small as 5 nm can be found to disperse on the surface of CNTs.

3.2. Electrochemical behavior

The cyclic voltammetric properties of the CNT–Ni nanocomposites and pure nickel are displayed in Fig. 2. In the case of pure nickel electrode, the anodic and cathodic peaks of the reversible redox reactions appear at 0.4 and 0.3 V, respectively. The anodic peak is related to α-$Ni(OH)_2$ and β-$Ni(OH)_2$ which oxidized to γ-NiOOH and β-NiOOH, while the cathodic peak is related to γ-NiOOH and β-NiOOH which oxidized to α-$Ni(OH)_2$ and β-$Ni(OH)_2$ (Fleischmann et al., 1971; Lo and Hwang, 1998). In the case of CNT–Ni nanocomposites, depending on the thickness of nickel coating, the oxidation peaks shift to 0.51–0.54 V while the cathodic reduction peaks shift to 0.18–0.16 V as the nickel thickness increased from 100 to 160 nm. The shifts of redox peak positions are in agreement with those reported in the literatures (Weng et al., 2004). In addition, the CNT–Ni nanocomposites consistently show larger anodic peak currents than the pure nickel electrode owing to the ultra nanonickel crystallites as shown in Fig. 1(d). Similar results have been reported (Weng et al., 2004). Consequently, the CNT–Ni nanocomposite structure indeed leads to a significant enhancement in sensor sensitivity due to enormous surface areas available for redox reactions, as compared to the plate-type nickel electrodes (Liao and Chou, 2000; Pang et al., 2001).

The operational potential window of the CNT–Ni nanocomposite electrode characterized by the limiting current range was obtained by the voltammetry linear sweep technique. As shown in Fig. 3, the applied potential on the CNT–Ni hybrid with 200 nm Ni thickness was swept from 0.46 to 0.65 V at a scan rate of 1 mV/s. It can be seen that for the potential window ranging from 0.49 to 0.55 V, the anodic current remained constant at 283 μA. This situation implies that the electrode response in this potential window was controlled by the steady-state mass transfer reaction. Consequently, the potential of 0.5 V was adapted as the working potential for the detection of ethanol concentration. It is known that nickel possesses different oxidation states including α-, β-, and γ-$Ni(OH)_2$/NiOOH in alkaline solutions (Schrebler Guzmán et al., 1978), and only the β-$Ni(OH)_2$/NiOOH has shown characteristic features in electrochemical catalysis (Sattar and Conway, 1969). In the present study, all of the CNT–Ni hybrid electrodes exhibited almost identical characteristics using the linear sweep voltammetry technique that was swept from 0.46 to 0.65 V at the scan rate of 1 mV/s.

3.3. Chronoamperometry

Fig. 4(a) shows the amperometric responses of the CNT–Ni nanocomposite biosensor with 200 nm Ni thickness. The amperometric response of the CNT–Ni biosensor upon each successive addition of 50 μM ethanol was recorded in a 0.5 M KOH aqueous solution at the operational potential of 0.5 V. With each addition of ethanol, the response time needed for reaching the 90% steady-state response was found to be ~10 s, which is far better than other reported values (Weng et al., 2004). Fig. 4(b) is the corresponding calibration curve. It is clearly observed that the amperometric response shows a linear relation to ethanol concentration for the concentration ranging from 50 to 600 μM.

The dependence of nickel thickness of the CNT–Ni biosensor on its sensitivity to ethanol concentration is presented in Fig. 5. In general, the sensitivity increases with increasing nickel thickness as the Ni thickness is ≤200 nm. As revealed in Fig. 1(c) and (d), nickel nanocrystallites disperse over the entire tube surface and provide enormous electrochemical active surface areas for redox reactions, thereby giving rise to the observed increase in sensitivity from 0.29 to 14.81 $\mu A\,\mu M^{-1}\,cm^{-2}$ as the nickel thickness increases from 60 to 200 nm. This performance is superior to those of other nickel-based electrodes reported previously (Liao and Chou, 2000; Pang et al., 2001; Weng et al., 2004). However, as the Ni thickness further increases to 240 nm, the sensitivity decreases to 12.75 $\mu A\,\mu M^{-1}\,cm^{-2}$. This decline in sensitivity can be attributed to the dense population of CNTs (Fig. S1; see Supporting Information), since the dense nature of CNTs may preclude the Ni particles of bigger size from entering into the inner space of CNTs. Thus, when too thick nickel (e.g. 240 nm) is deposited, the major Ni particles would agglomerate on the tip of CNTs and a

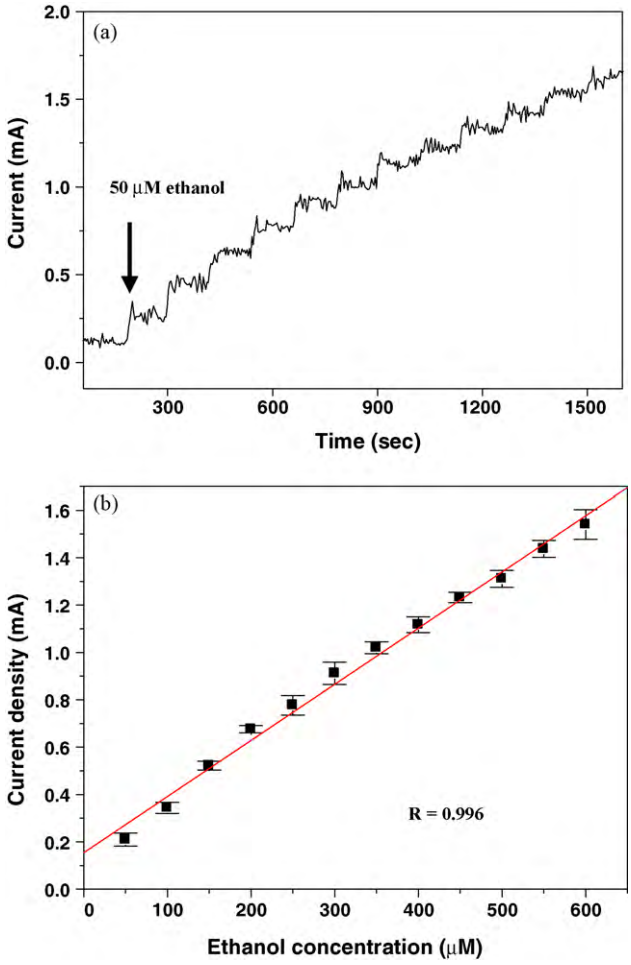

Fig. 4. (a) Amperometric responses and (b) the calibration plot of the CNT–Ni nanocomposite with 200 nm Ni thickness to successive additions of 50 μM ethanol at a potential of 0.5 V in 0.5 M KOH solution. Each response in (b) represents the mean ± S.D. of five determinations.

point would be reached that the CNTs is covered by a nickel film (Fig. S2; see Supporting Information). Under such a situation, the hybrid behaves more like a two-dimensional plate-type nickel electrode, which has significantly decreased surface areas available for

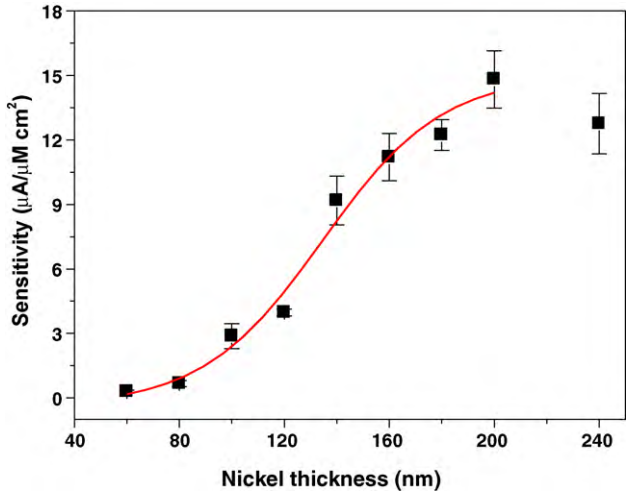

Fig. 5. Effect of e-beam deposited nickel thickness on sensitivity of ethanol sensing. Each response represents the mean ± S.D. of five determinations.

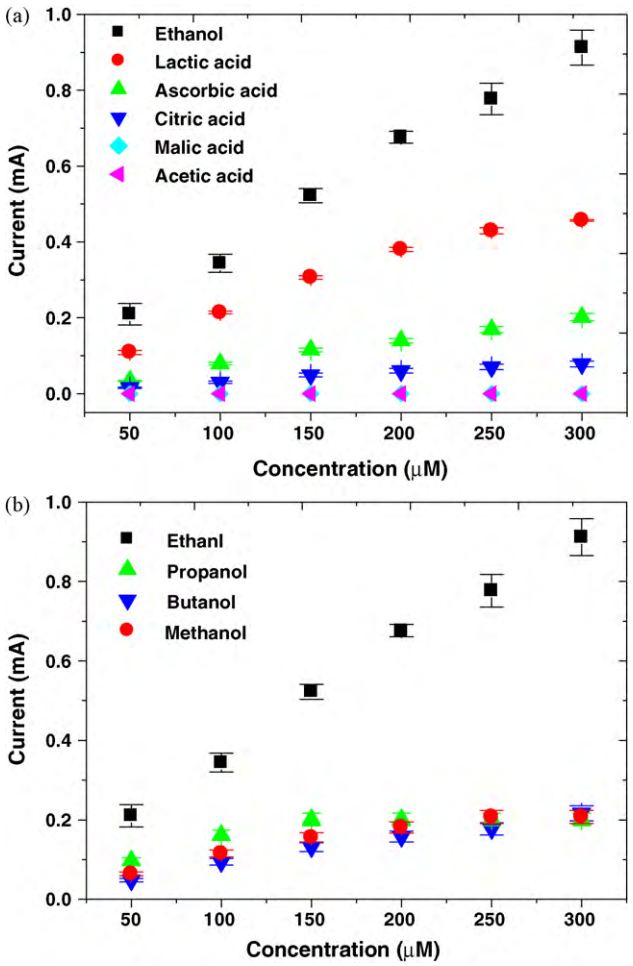

Fig. 6. Calibration plots of the CNT–Ni nanocomposite with 200 nm Ni thickness to successive additions of 50 μM ethanol and potential interfering species: (a) ethanol, lactic acid, ascorbic acid, citric acid, malic acid, and acetic acid; (b) ethanol, methanol, propanol, and butanol. Sensing condition: applied potential 0.5 V vs. Ag/AgCl; 0.5 M KOH electrolyte. Each response represents the mean of five (for ethanol) or three (for interfering species) experiments, with a relative standard deviation (R.S.D.) lower than 5.16, 1.46, 4.62, 9.76, NA (not available), NA, 7.78, 7.85, and 8.64% for ethanol, lactic acid, ascorbic acid, citric acid, malic acid, acetic acid, methanol, propanol, and butanol, respectively.

sensing compared to the CNT–Ni nanocomposite electrode. Therefore, the amount of nickel loading on the CNTs needed to obtain the highest sensitivity is determined by varying the thickness of the deposited nickel till an optimum surface coverage is reached for nickel nanocrystallite attachments.

3.4. Selectivity of the sensor

The selectivity of the sensor was examined by studying the amperometric responses of the sensors to successive additions of 50 μM of ethanol and eight potential interfering species, namely lactic acid, ascorbic acid, citric acid, malic acid, acetic acid, methanol, propanol, and butanol. All amperometric measurements were carried out in a 0.5 M KOH aqueous solution at an operational voltage of 0.5 V. Fig. 6(a) displays the corresponding calibration curves for ethanol and the five acids. Clearly, the amperometric trend in sensitivity was observed in the following order: ethanol > lactic acid > ascorbic acid > citric acid > malic acid = acetic acid. Furthermore, it is noted that the biosensor exhibited essentially negligible responses to all interfering species except lactic acid. The calibration curves for ethanol, methanol, propanol, and butanol are shown in Fig. 6(b). Obviously, the sensor exhibited a

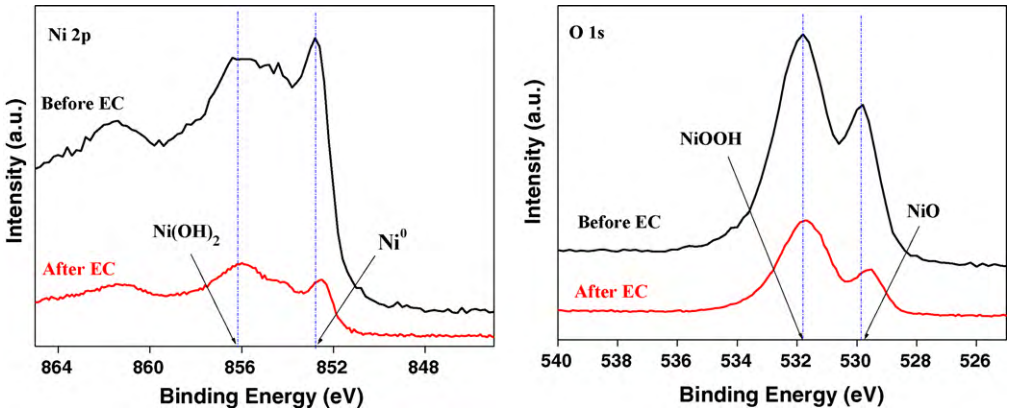

Fig. 7. HRXPS spectra of Ni 2p and O 1s of the CNT-Ni hybrid before and after EC sensing of ethanol.

much higher sensitivity toward ethanol than other alcohols, and is suitable for use in both medical and brewing applications. Two factors, the oxidation overpotential and the molecular structure, can affect the selectivity of ethanol sensors. The working overpotential utilized in this study is 0.5 V at which other alcohols may oxidize, too. However, the different molecular structure associated with each interfering species may render a different reaction rate as it undergoes each of the cyclic reactions, i.e., changes of functional groups from ethanol, aldehyde to carboxylic acid (Pang et al., 2001), at the hybrid electrode. Thus, although the chemical structure of each alcohol has a hydroxyl group, the hybrid electrode may exhibit a different level of response current to each alcohol determination. Based on the data shown in Fig. 6(b), we may conclude that the overall reaction rate of each alcohol is in the following order: ethanol > methanol = propanol = butanol.

Relative errors on the determination of 300 μM ethanol in solution caused by the same concentration of lactic acid, ascorbic acid, citric acid, malic acid, acetic acid, and other alcohols are 50.1%, ≤22.2%, ~8.6%, 0%, 0%, and ~23.7%, respectively. The large errors caused by the lactic acid, ascorbic acid, and alcohols may be due to the relatively high operating potential of the electrode (+0.5 V).

3.5. HRXPS analysis and stability of the sensor performance

The ethanol detection mechanism of nickel-based electrodes has been widely studied (Sattar and Conway, 1969; Carbonio et al., 1982; Lo and Hwang, 1995; Liao and Chou, 2000), which relied upon the oxidation of ethanol by the redox pair of $Ni(OH)_2$/NiOOH on nickel surface in alkaline media. To confirm this, we have employed high-resolution XPS to investigate the states of $Ni(OH)_2$/NiOOH before and after electrochemical (EC) sensing of ethanol. The HRXPS spectra and their assignments are shown in Fig. 7. Prior to EC sensing, the Ni 2p and O 1s spectra of the hybrid show the characteristic peak of the $Ni(OH)_2$ bond at 856.2 eV and an oxygen related peak at 531.8 eV contributed by NiOOH attached to the surface of CNTs, respectively. After EC sensing, the Ni 2p and O 1s spectra exhibit similar while declining features with negligible shifts in the binding energies of the redox pair. The lower intensity of the redox pair after EC sensing is due to the aggregation of CNTs in alkaline media, which results in less active surface areas for redox reactions.

The time interval between the two HRXPS measurements, i.e., prior to and after EC sensing of ethanol, was ~2 months. This HRXPS analysis not only illustrates the existence of $Ni(OH)_2$/NiOOH by oxidation of ethanol but also indicates the long-term stability of the sensor with respect to its shelf-life (not in use). The long-term working stability of the sensor was also studied by performing a 20-day continuous measurement. The result shows that the sensor could still produce >90% of its initial response to 50 μM ethanol on the 20th day and the day-to-day variation in sensitivity is ~5%.

Table 1
Results for the determination of ethanol concentration in red wine using the CNT–Ni nanocomposite sensor with 200 nm Ni thickness.

	Sample no.	
	1	2
Nominal value[a] (μM)	50	100
This work[b] (μM)	49.4 ± 2.6	99.8 ± 5.6

[a] Calculated from the volume concentration shown on the product level of the wine sample.
[b] Mean ± S.D. of five measurements.

3.6. Reproducibility of the sensor

The proposed sensor fabrication condition allows the reproducible production of ethanol sensors. To assess this, six more CNT–Ni hybrid electrodes have been prepared under otherwise the same conditions, i.e., 200 nm Ni loading. The performances of these sensors were tested by applying them to the determination of the concentration in alcoholic beverages: beer and wine. The responses obtained with the biosensors showed a relative error of within 6%, indicating the reproducibility of the fabrication.

3.7. Real sample analysis

The CNT–Ni biosensor with 200 nm Ni thickness was used for the measurement of ethanol concentration in red wine. The alcohol volume concentration shown on the product level of the wine sample is 12%. The sample solution was first diluted with deionized water and used as stock substrate solutions. The change in current density was monitored after the addition of a certain amount of the diluted red wine to the reaction cell. The concentration contributed to the measured signal was estimated by using the calibration curve as shown in Fig. 5(b). The assay results determined by this sensor are shown in Table 1. It can be seen that the result showed an acceptable correlation between the claimed and measured values.

4. Conclusions

In summary, we have demonstrated a simple and efficient approach for the fabrication of ethanol biosensors based on nickel nanoparticles modified MWCNT arrays grown directly on Si substrates. The Ni nanoparticles obtained by e-beam deposition were well-dispersed on the sidewalls of CNTs, which consequently showed enhanced electrocatalytic activity in ethanol oxidation reactions compared to the plate-type Ni electrodes. The sensitivity

of the sensor generally increases with increasing nickel thickness till an optimum surface coverage of nickel nanocrystallites on CNTs is reached. The optimal Ni thickness is about 200 nm and the resulting CNT–Ni nanocomposite exhibited a sensitivity of $14.81 \pm 1.33\ \mu A\ \mu M^{-1}\ cm^{-2}$.

Acknowledgement

This work has been supported by the National Science Council of Taiwan under Grant No. 95-2112-M-007-026-MY3.

Appendix A. Supplementary data

Supplementary data associated with this article can be found, in the online version, at doi:10.1016/j.bios.2010.06.016.

References

Arai, S., Endo, M., Kaneko, N., 2004. Carbon 42, 641–644.
Carbonio, R.E., Macango, V.A., Giordano, M.C., Vilche, J.R., Arvia, A.J., 1982. J. Electrochem. Soc. 129, 983–991.
Fang, W.-C., Chyan, O., Sun, C.-L., Wu, C.-T., Chen, C.-P., Chen, K.-H., Chen, L.-C., Huang, J.-H., 2007. Electrochem. Commun. 9, 239–244.
Fleischmann, M., Korinek, k., Pletcher, D., 1971. J. Electrochem. Soc. 31, 39–49.
Huang, J.H., Chen, Y.S., Chuang, C.C., Wong, Y.M., Kang, W.P., 2005. J. Vac. Sci. Technol. B 23, 805–808.
Jin, G.-P., Ding, Y.-F., Zheng, P.-P., 2007. J. Power Sources 166, 80–86.
Katrlik, J., Svorc, J., Stredansky, M., Miertus, S., 1998. Biosens. Bioelectron. 13, 181–191.
Kim, H.-S., Lee, H., Han, K.-S., Kim, J.-H., Song, M.-S., Park, M.-S., Lee, J.-Y., Kang, J.-K., 2005. J. Phys. Chem. B 109, 8983–8986.
Lee, C.H., Wang, S.C., Yuan, C.J., Wen, M.F., Chang, K.S., 2007. Biosens. Bioelectron. 22, 877–884.
Liao, Y.Y., Chou, T.C., 2000. Electroanalysis 12 (1), 55–59.
Lim, S.H., Wei, J., Lin, J., Li, Q., You, J.K., 2005. Biosens. Bioelectron. 20, 2341–2346.
Liu, Q., Lu, X., Li, J., Yao, X., Li, J., 2007. Biosens. Bioelectron. 22, 3203–3209.
Lo, Y.L., Hwang, B.J., 1995. J. Electrochem. Soc. 142, 445–450.
Lo, Y.L., Hwang, B.J., 1998. Langmuir 14, 944–950.
Luo, X., Morrin, A., Killard, A.J., Smyth, M.R., 2006. Electroanalysis 18, 319–326.
Manso, J., Mena, M.L., Yáñez-Sedeño, P., Pingarrón, J., 2007. J. Electroanal. Chem. 603, 1–7.
Nugent, J.M., Santhanam, K.S.V., Rubio, A., Ajayan, P.M., 2001. Nano Lett. 1, 87–91.
Pang, C.C., Chen, M.H., Lin, T.Y., Chou, T.C., 2001. Sens. Actuators B 73, 221–227.
Sattar, M.A., Conway, B.E., 1969. Electrochim. Acta 14, 695–710.
Schrebler Guzmán, R.S., Vilche, J.R., Arvía, A.J., 1978. J. Appl. Electrochem. 8, 67–70.
Vijayakumar, A.R., Csoregi, E., Heller, A., Gorton, L., 1996. Anal. Chim. Acta 327, 223–234.
Wang, F., Arai, S., Endo, M., 2005. Carbon 43, 1716–1721.
Wang, J., 2005. Electroanalysis 17, 7–14.
Wang, J., Gonzalez-Romero, E., Ozsoz, M., 1992. Electroanalysis 4, 539–544.
Weng, Y.C., Rick, J.F., Chou, T.C., 2004. Biosens. Bioelectron. 20, 41–51.
Xie, X., Suleiman, A.A., Guilbault, G., Yang, Z., Sun, Z., 1992. Anal. Chim. Acta 266, 325–329.
Tang, H., Chen, J., Yao, S., Nie, L., Deng, G., Kuang, Y., 2004. Anal. Biochem. 331, 89–97.